

## Analysis of Dual-Mode Lasing Characteristics in a 1310 nm Optically-Injected Quantum Dot Distributed Feedback Laser

R. Raghunathan<sup>1,3,\*</sup>, J. Olinger<sup>1</sup>, A. Hurtado<sup>2</sup>, F. Grillot<sup>3</sup>, V. Kovanis<sup>1,4</sup>, and L. F. Lester<sup>1</sup>

<sup>1</sup>Bradley Department of Electrical and Computer Engineering, Virginia Polytechnic Institute and State University, 302 Whittemore Hall, Blacksburg Virginia, 24061, USA

<sup>2</sup>Institute of Photonics, University of Strathclyde, Wolfson Centre, 106 Rottenrow East, Glasgow, G4 0NW, Scotland, United Kingdom

<sup>3</sup>Telecom Paristech, Ecole Nationale Supérieure des Télécommunications, CNRS LTCI, 75634 Paris Cedex 13, France

<sup>4</sup>Nazarbayev University, 53 Kabanbay Batyr Ave., Astana 010000, Kazakhstan

### ABSTRACT

Recent work has shown the Quantum Dot (QD) material system to be well-suited to support dual-mode lasing. In particular, optical injection from a master laser (ML) into the residual Fabry-Perot (FP) modes of a 1310 nm Quantum Dot Distributed Feedback (QD-DFB) laser has been recently demonstrated to offer a highly reliable platform for stable dual-mode lasing operation. External controls on the ML, such as operating temperature and bias current, can be used to precisely adjust the spacing between the two lasing modes. This tunability of mode-separation is very promising for a range of applications requiring the generation of microwave, millimeter wave and terahertz signals. Considering the versatility and utility of such a scheme, it is imperative to acquire a deeper understanding of the factors that influence the dual-mode lasing process, in order to optimize performance. Toward this end, this paper seeks to further our understanding of the optically-injected dual-mode lasing mechanism. For fixed values of optical power injected into each FP residual mode and wavelength detuning, the dual-mode lasing characteristics are analyzed with regard to important system parameters such as the position and the intensity of the injected residual mode (relative to the Bragg and the other residual FP modes of the device) for two similarly-fabricated QD-DFBs. Results indicate that for dual mode lasing spaced less than 5 nm apart, the relative intensity of the injected FP mode and intracavity noise levels are critical factors in determining dual mode lasing behavior. Insight into the dual-mode lasing characteristics could provide an important design guideline for the master and QD-DFB slave laser cavities.

**Keywords:** Dual-mode lasing, Optical injection, Quantum dot lasers, Distributed feedback lasers.

### 1. INTRODUCTION

The inherent benefits that coherent photonic RF sources could potentially offer over conventional electronic sources, such as ultrahigh carrier frequencies, very wide bandwidths, immunity to conduction losses and electromagnetic interference (EMI) during transmission, and lower energy consumption with the resulting benefit of lowered costs have led to a tremendous interest of late in the development of photonically-generated RF, microwave, mm-wave and THz sources.<sup>1</sup> Consequently, in the past few years, several techniques for the photonic generation of RF signals with a high spectral purity have been developed, such as mode-locking<sup>2</sup>, optical frequency combs<sup>3</sup>, optical heterodyning<sup>4</sup> and sideband optical injection<sup>5,6</sup>.

More recently, sideband optical injection into a laterally loss-coupled QD-DFB laser was shown to induce stable dual-mode lasing in such a device, such that two stable lasing modes are simultaneously generated within the same cavity. Extensive work by A. Hurtado et al has shown that with a relatively simple Master-Slave injection locking setup comprised of easily available optical components, external controls on the Master Laser (ML) such as operating temperature and bias current can be used to precisely adjust the spacing between the two lasing modes, thereby enabling a single, tunable source to generate a range of difference frequencies in the optical domain.<sup>7-9</sup>

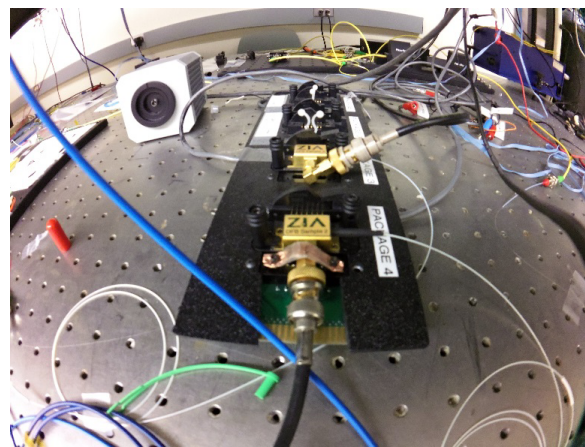
\*[raghunat@vt.edu](mailto:raghunat@vt.edu); Phone: (540) 231-6646; Fax: (540) 231-3362

Furthermore, QD media have been shown to possess numerous properties that could potentially make QD lasers vastly more desirable than bulk or quantum well (QW) devices.<sup>10</sup> Some of these properties include significantly lower threshold currents<sup>11</sup>, lower levels of amplified spontaneous emission (ASE)/intracavity noise<sup>12</sup> and lower linewidth enhancement factors close to threshold<sup>13</sup> (promising for chirp-reduction in the generated signals).

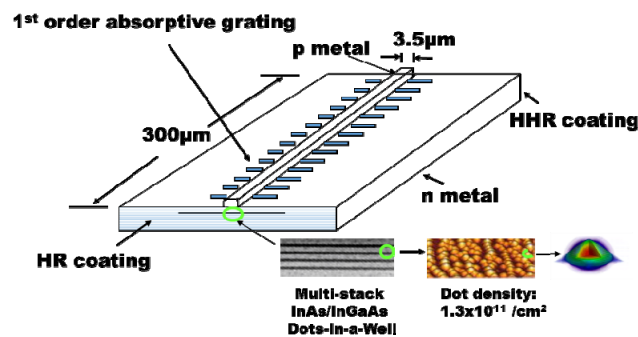
These superior properties of the QD material system, combined with the demonstration of the optically-injected QD-DFB as a highly tunable dual-mode laser source suitable for a wide range of RF-Photonic applications necessitate a more precise and in-depth understanding of the key factors that impact/influence the dual-mode lasing process. Toward this end, and in order to optimize performance and guide future device design, this work seeks to further our understanding of the dual-mode lasing mechanism.

## 2. DEVICE STRUCTURE AND EXPERIMENTAL SETUP

The basic structure investigated in this study is a laterally loss-coupled QD-DFB laser. Two devices (fabricated identically) were characterized to enable an expanded set of data, in order to get a better sense of device behavior. A photograph and schematic of the devices are shown in Fig. 1.



a.)

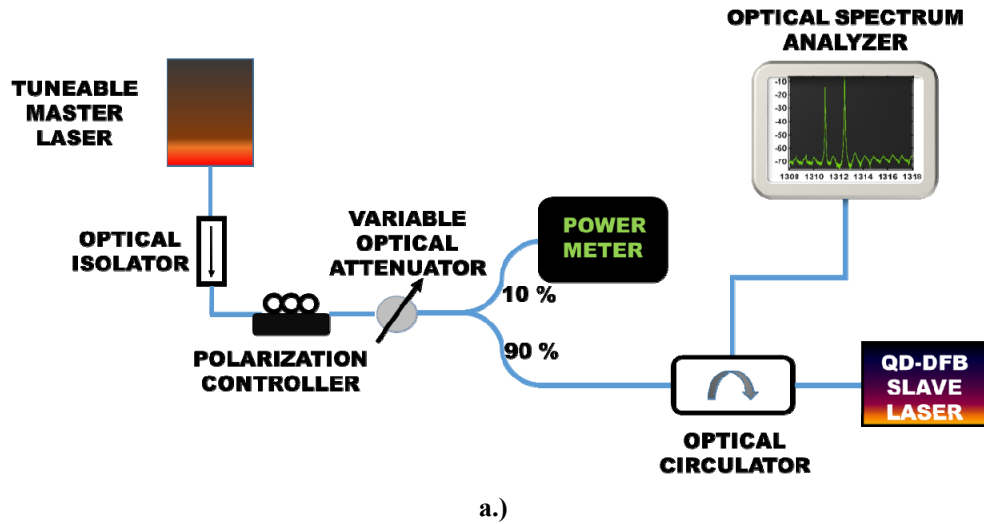


b.)

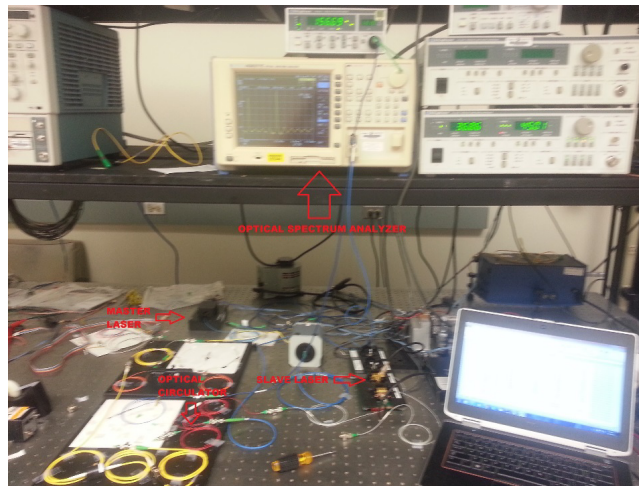
**Fig. 1:** a.) Photograph of packaged QD-DFBs on mount, and b.) Schematic of cavity layout/construction.

The dots-in-a-well (DWELL) laser structure is grown by solid source molecular beam epitaxy on a (001) GaAs substrate, with a typical single layer areal dot density  $\sim 1.3$  to  $2.4 \times 10^{11} \text{ cm}^{-2}$ . Each device is fabricated starting with a  $3.5 \mu\text{m}$  ridge, followed by the e-beam lithographic patterning and liftoff of the lateral absorptive metal grating to form a laterally cross-coupled DFB laser. Complete details of the fabrication procedure may be found elsewhere<sup>14</sup>. The gratings are comprised of a metal such as Chromium, and have a period of 200 nm. Each laser cavity has a length of  $300 \mu\text{m}$  and the end facets are asymmetrically HR/HHR coated, which enables a lower threshold, higher Q-factor and output predominantly from one facet.

The experimental setup for this experiment follows our previous work<sup>7-9</sup>. Fig. 2 shows a schematic and a photograph of the same.



a.)



b.)

**Fig. 2a.)** Schematic of the experimental setup (blue lines indicate optical fiber), and **b.)** Photograph of the setup, with key components labelled in red.

A 1310 nm quantum well DFB laser acts as the “Master” laser (ML), injecting light into the 1310 nm QD-DFB “Slave” laser (SL). As mentioned in our earlier publications, the ML uses temperature-control for coarse-tuning to enable injection at a desired wavelength closest to the SL residual mode, and current-control to achieve the fine-tuning necessary to set its injection wavelength to a desired detuning relative to the slave side-mode being injected. A polarization controller is used to set the polarization of the output from the ML, while a variable optical attenuator enables control over the power injected into the SL. A 90-10 optical coupler is used to split the signal into two arms, where the 90% arm is injected into the SL via an optical circulator, while the 10% arm is used to monitor the strength of the injected signal. The output reflected from the QD-DFB laser is analyzed using an optical spectrum analyzer.

### 3. EXPERIMENTAL RESULTS

Fundamentally, the optically-injected Dual-Mode laser relies on stable locking between the ML and the SL modes. Consequently, optimizing device design and performance requires an in-depth understanding of the instabilities that interfere with the Master-Slave locking process.

Toward this end, the experiments in this work were setup to closely study the dual-mode lasing characteristics for a number of different side-modes of the QD-DFB laser. To allow for possible variations in device behavior as a result of fabrication process inhomogeneities, two different QD-DFBs (designated #1 and #2) with nominally similar designs and identical fabrication recipes were analyzed. The experimental methodology was as follows. In order to compare lasing characteristics for all injected side-modes under the same operating conditions, the temperature of the SL was fixed at a given value. The ML was temperature-tuned to enable optical injection into the different side-modes. However, given that the separation between the adjacent Fabry-Perot modes of the SL was 0.8 nm, safe operating temperatures for the ML meant that a maximum of 6 adjacent modes could be injected into. Consequently, lasing characteristics are analyzed in detail for two separate sets of modes in this work – i.) 6 successive side-modes on the long wavelength side of the Bragg mode of the QD-DFB, and ii.) 3 successive side-modes on either side of the Bragg mode of the QD-DFB. Further, keeping the optical power injected into each Fabry-Perot (F-P) residual/side mode fixed at 1 mW and a fixed wavelength detuning of  $\Delta\lambda = |\lambda_{ML} - \lambda_{residual}| = 0$ , the dual-mode lasing characteristics were obtained by plotting for each injected side-mode, the difference of the intensities of the injected side-mode and the Bragg mode as a function of the QD-DFB bias current, and analyzed with respect to key parameters such as the position and the intensity of the injected side-mode (relative to the Bragg and other side-modes of the device).

Fig. 3 plots the L-I characteristic of QD-DFB #1, operated in the solitary configuration at a temperature of 40 °C. Threshold was observed at 6.16 mA.

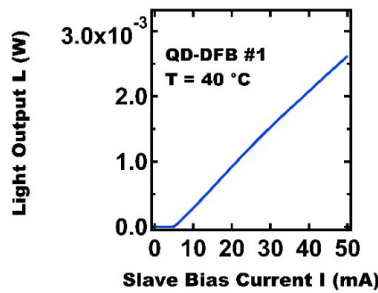
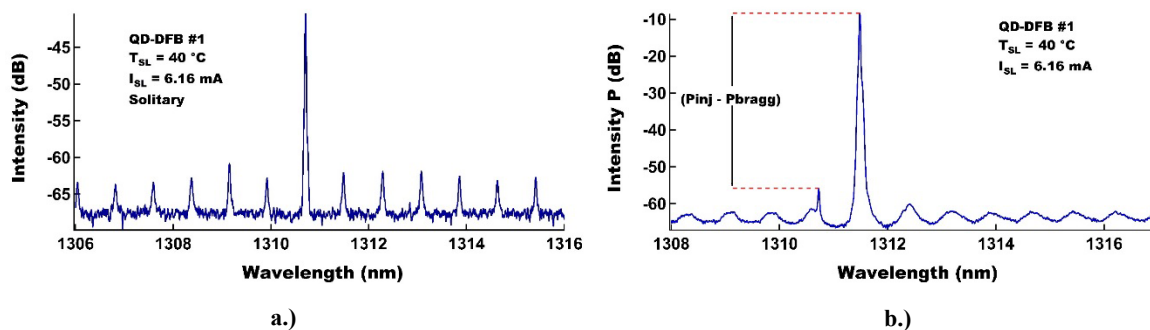
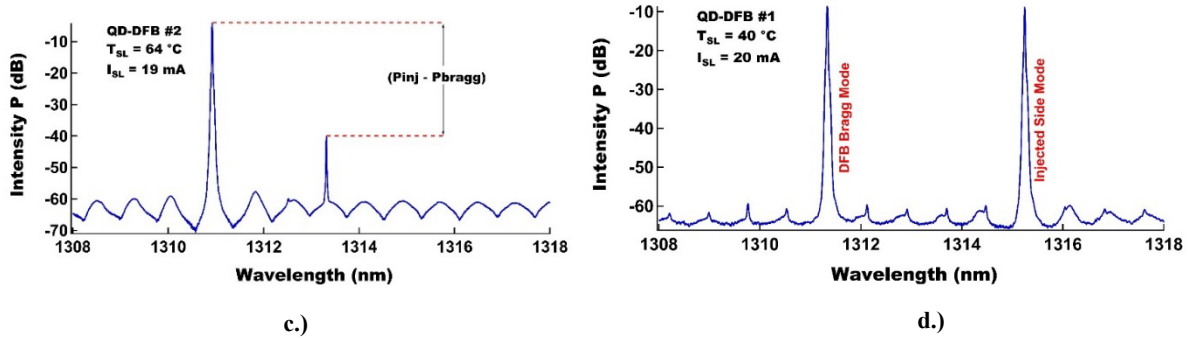


Fig. 3: L-I Characteristic for QD-DFB #1 at 40 °C. Threshold occurs at 6.16 mA.

The corresponding solitary mode-structure of the device in solitary operation (i.e., no external optical injection) is shown in Figure 4a. Depending on the solitary SL power relative to the injection strength, 3 typical operating states were observed – i.) strong suppression of the Bragg mode by the injected side-mode at low SL bias conditions near threshold (Fig. 4b), ii.) partial suppression of the Bragg mode for intermediate bias levels on the SL (Fig. 4c), and iii.) negligible suppression of the Bragg mode, i.e. Dual-Mode lasing (Fig. 4d). Notice the degradation in the structure of side-modes as light is injected into the SL.





**Fig. 4:** Measured optical spectra, **a.**) solitary device (QD-DFB #1) at threshold (40°C), **b.**) strong suppression of Bragg mode (QD-DFB #1) under external optical injection at threshold (40°C), **c.**) partial suppression of Bragg mode (QD-DFB #2) at a bias current of 19 mA (64°C), and **d.**) dual-mode lasing (QD-DFB #1) at a bias current of 20 mA (40°C).

**Table I:** Measured dual-mode intensity differences for the first 6 successive side-modes on the long wavelength side of the Bragg mode (QD-DFB #1 at 40°C). Power of the injected residual mode is denoted  $P_{Inj, Res\#}$ .

SLAVE BIAS CURRENT (mA)	$(P_{Bragg} - P_{Inj, Res1})$ (dB)	$(P_{Bragg} - P_{Inj, Res2})$ (dB)	$(P_{Bragg} - P_{Inj, Res3})$ (dB)	$(P_{Bragg} - P_{Inj, Res4})$ (dB)	$(P_{Bragg} - P_{Inj, Res5})$ (dB)	$(P_{Bragg} - P_{Inj, Res6})$ (dB)
6.16	-47.45	-47.09	-45.93	-46	-47.13	-47
6.5	-45.5	-44.8	-44.5	-43.85	-45.64	-44.5
6.75	-44	-43.5	-43	-42.9	-44.25	-43.65
7	-43.5	-42.5	-41.75	-41.85	-43.25	-42
7.25	-40.75	-40.7	-39.4	-40.6	-41.4	-39.5
7.5	-38.7	-39	-37.5	-38.2	-39	-37.5
7.75	-34	-34.5	-20.5	-37.7	-35.5	-16.75
8	-32	-21	-14.28	-34.5	-15.6	-16.7
8.25	-19.26	-14	-12.25	-29.5	-15.5	-12.75
8.5	-13.47	-13.25	-10.05	-14	-14.15	-12
8.75	-11.5	-11.25	-9	-12.15	-10	-11.6
9	-10.75	-10.7	-8.5	-9.35	-10	-9.1
9.5	-7.5	-7.85	-6.75	-7.58	-8.5	-6.85
10	-8	-7.35	-5.9	-7.3	-7.15	-6.2
12.5	-4.85	-4	-2.25	-3.7	-3.7	-3
15	-2.65	-1.8	-0.1	-1.75	-1.7	-0.8
17.5	-1.5	-0.31	0.9	-1.25	-0.75	-0.25
20	-0.36	1	0.45	-0.43	0.25	0

The first experiment involved injection into the first 6 successive side-modes on the long wavelength side of the Bragg mode of QD-DFB #1. The difference of the powers measured for the Bragg mode and the injected side-modes as a function of the SL bias current is tabulated in Table I and plotted in Fig. 5.

A careful comparison of the values in the six columns corresponding to the differences in the intensities of the two dominant modes shows a more or less similar evolution with increasing slave bias current. A slight deviation from this trend can be seen between a slave bias current of 7.75 mA – 8.25 mA, when residual modes 3 and 6 show a more drastic reduction in the intensity difference compared to the other side modes, while residual modes 1 and 4 show a more sluggish reduction in the same. This can be quickly noticed in Fig. 5, where the traces corresponding to side-modes 3 and 6 (orange inverted solid triangles and black crosses, respectively) show the onset of Dual-Mode threshold at about 7.75 mA, while the traces corresponding to side-modes 1 and 4 (red solid circles and blue solid diamonds, respectively) show the same closer to 8.25 mA. Side-modes 2 and 5 (solid brown triangles and solid green squares, respectively) show a threshold very close to 8 mA. This slight difference of the onset of Dual-Mode threshold was seen to coincide with a slight fluctuation in the associated side-mode intensities. It was observed that for slave current values in the range 7.75 mA – 8.25 mA, side-modes 1 and 4 were most intense, while side-modes 3 and 6 were the weakest, with the intensities of side-modes 2 and 4 somewhere in-between. Simply put, the more intense side-modes required a slightly higher slave bias to reach threshold. Beyond about 8.5 mA, all the injected side-modes again showed a similar evolution, and stable dual-mode lasing with almost identical lasing mode intensities was observed in all cases by a slave bias of 20 mA.

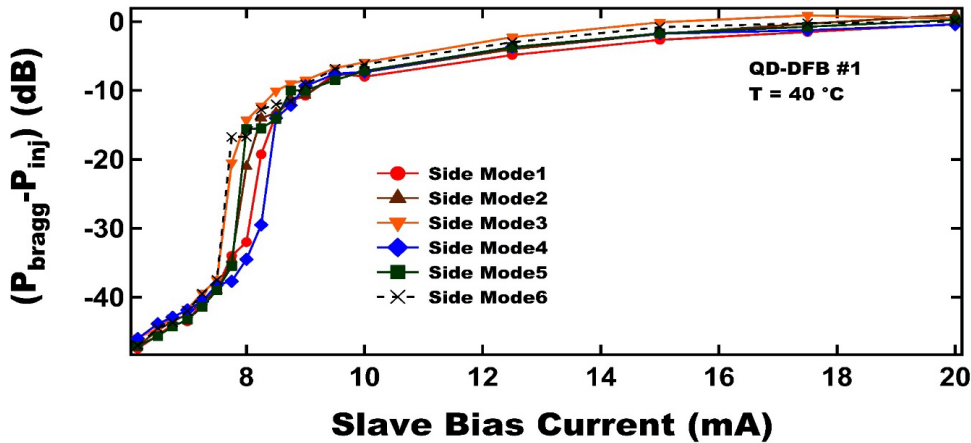


Fig. 5: Measured dual-mode intensity difference characteristics for the first 6 successive side-modes on the long wavelength side of the Bragg mode (QD-DFB #1 at 40 °C).

The 3 typical operating states of the optically-injected QD-DFB mentioned earlier can be clearly seen from Fig. 5 – strong suppression of the Bragg mode occurred for all injected side-modes in the ‘tail’ of the plot, up to a slave current of 7.75 mA, partial suppression of the Bragg mode was observed during the sharp transition in the vertical segments between 7.75 mA and 8.25 mA, while the leveling-off of all curves at the top of the plot corresponds to a diminishing difference between the two lasing peaks, eventually leading to two modes of nearly identical intensity.

Next, the same experiment was repeated on QD-DFB #2, so that the 6 consecutive modes on the long wavelength side were subjected to external optical injection. The L-I curve for the device shows a threshold at 9 mA (Fig. 6). The higher threshold for this device suggests the likelihood of more intra-cavity noise.

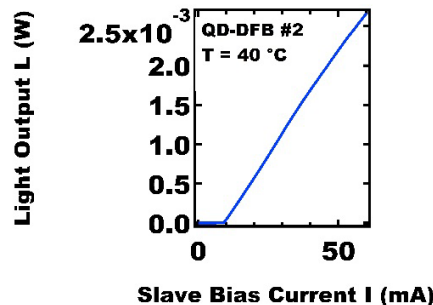
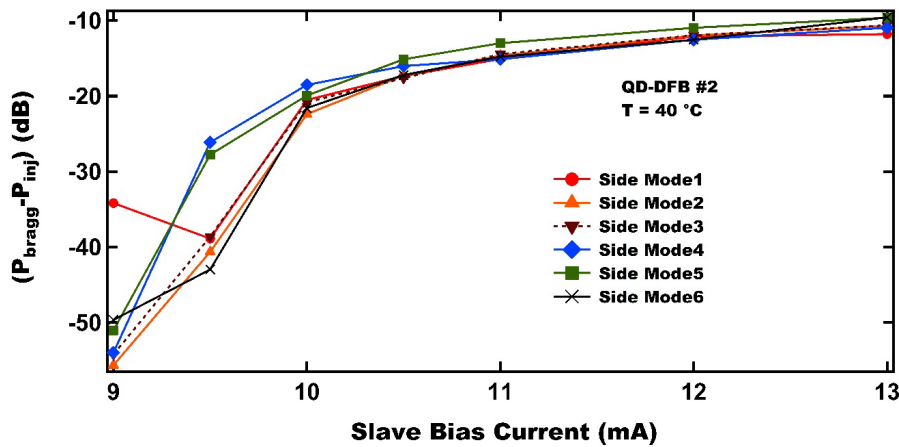


Fig. 6: L-I Characteristic for QD-DFB #2 at 40 °C. Threshold occurs at 9 mA.

A reduced dataset is shown in Table II to highlight the main trends, and plotted in Fig. 7.

**Table II:** Measured dual-mode intensity differences for the first 6 successive side-modes on the long wave-length side of the Bragg mode (QD-DFB #1 at 40 °C). Power of the injected residual mode is denoted  $P_{Inj, Res\#}$ .

SLAVE BIAS CURRENT (mA)	$(P_{Bragg} - P_{Inj, Res1})$ (dB)	$(P_{Bragg} - P_{Inj, Res2})$ (dB)	$(P_{Bragg} - P_{Inj, Res3})$ (dB)	$(P_{Bragg} - P_{Inj, Res4})$ (dB)	$(P_{Bragg} - P_{Inj, Res5})$ (dB)	$(P_{Bragg} - P_{Inj, Res6})$ (dB)
9	-34.18	-55.66	-54.23	-53.98	-51.04	-49.65
9.5	-38.88	-40.64	-38.62	-26.12	-27.76	-42.98
10	-20.51	-22.4	-20.82	-18.52	-19.93	-21.59
10.5	-17.34	-17.26	-17.63	-16.03	-15.13	-17.21
11	-15.09	-14.63	-14.43	-15.12	-13	-14.79
12	-12.12	-11.98	-11.95	-12.54	-10.96	-12.54
13	-11.78	-10.69	-10.65	-10.95	-9.62	-9.57



**Fig. 7:** Measured dual-mode intensity difference characteristics for the first 6 successive side-modes on the long wavelength side of the Bragg mode (QD-DFB #2 at 40 °C).

The trends observed from the plots in Fig. 7 are largely similar to those in Fig. 5. The main differences were observed just above threshold, between 9 mA and 9.5 mA, where injected side-modes 1 and 6 (red solid circles and black crosses, respectively) showed some fluctuations in the relative intensities of the injected side-modes relative to the Bragg mode. In the same bias range, it was observed that injection into side-modes 4 and 5 (blue solid diamonds and green solid squares, respectively) lead to the Bragg mode being less suppressed, and the two-mode state exhibiting fewer fluctuations in their relative intensities.

In this case, the solitary mode-structure of the QD-DFB SL showed that near threshold, side-modes 4 and 5 were the weakest (least intense), while side-mode 1 exhibited significant fluctuations in its intensity and structure. However, all injected side-modes showed a similar trend above a SL bias current of 10 mA, with the intensity-difference between the two lasing modes diminishing.

The third part of the experiment involved investigating the Dual-Mode characteristics for injected side-modes on both the long and short wavelength sides of the Bragg mode under the same conditions. As mentioned previously, the temperature tuning on the ML required to inject into side-modes on either side of the central Bragg mode limited the dynamic range of the ML to a maximum of 3 side-modes on either side of the Bragg mode, in order to ensure safe operating conditions.

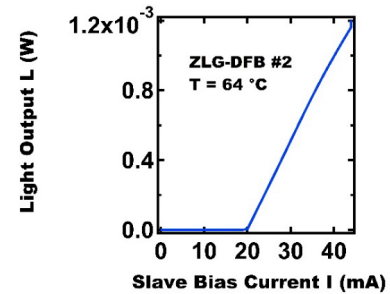


**Fig. 8:** L-I Characteristic for QD-DFB #2 (64 °C). Threshold occurs at 19 mA.

Thus, in order to enable the ML emission wavelength to be tuned to span this range of side-mode wavelengths, the SL had to be set at an operating temperature of 64 °C. The L-I characteristic for the solitary QD-DFB at 64 °C is shown in Fig. 8. Threshold occur at a SL bias of 19 mA. In Table III and Fig. 9 below, the three side-modes on the lower wavelength side of the Bragg mode are designated -3, -2 and -1 (with -3 referring to the shortest wavelength), whereas the three side-modes on the long wavelength side are marked +1, +2 and +3 (with +3 corresponding to the longest wavelength).

**Table III:** Measured dual-mode intensity differences for the first 3 successive side-modes on the short (col. 2-4) & long (col. 5-7) wavelength side of the Bragg mode (QD-DFB #2 at 64°C). Power of injected residual mode is denoted  $P_{Inj, Res\#}$ .

SLAVE BIAS CURRENT (mA)	( $P_{Bragg} - P_{Inj, Res-3}$ ) (dB)	( $P_{Bragg} - P_{Inj, Res-2}$ ) (dB)	( $P_{Bragg} - P_{Inj, Res-1}$ ) (dB)	( $P_{Bragg} - P_{Inj, Res+1}$ ) (dB)	( $P_{Bragg} - P_{Inj, Res+2}$ ) (dB)	( $P_{Bragg} - P_{Inj, Res+3}$ ) (dB)
19	-36	-37.5	-42.75	-35.65	-33.11	-38.7
19.25	-36	-40.5	-44.85	-27.25	-28.75	-37
19.5	-32.5	-40.15	-44.8	-26.15	-32	-39.5
19.75	-39.25	-41.5	-46.25	-25.5	-26.44	-35
20	-36	-35	-46	-23.75	-24.75	-27.25
20.25	-25	-28.75	-42	-22.75	-22.7	-24.3
20.5	-24.5	-29.25	-42	-23.73	-23.5	-23
25	-14.25	-15.5	-18.05	-20	-22.62	-22.55
27.5	-10.14	-11.16	-12	-13.85	-15.65	-14.7
30	-7.75	-9.1	-7.45	-8.85	-9.3	-13.5
32.5	-4.37	-6.4	-7.25	-6	-6.25	-9.5
35	-4.35	-4.3	-4.63	-4	-4.5	-6.4

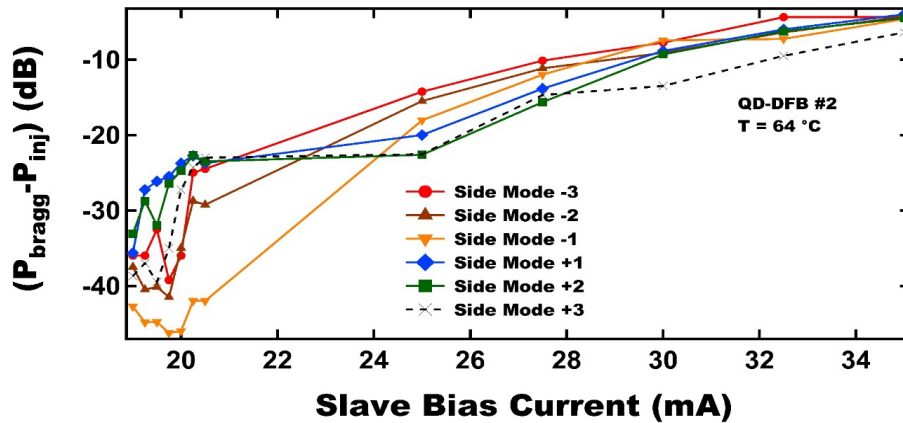


**Fig. 9:** Measured dual-mode intensity difference characteristics for the first 3 successive side-modes either side of the Bragg mode (QD-DFB #2 at 64°C). Side-modes on the long wavelength side of the Bragg mode are labelled with a “+” sign, while side-modes on the short wavelength side are labelled with a “-” sign, with -/+ 3 denoting the shortest/longest wavelength.

As can be seen clearly, the data recorded in Table III and the plots in Fig. 9 are at variance with the previous two cases of injection into the first 6 successive side-modes on the long wavelength side of the Bragg mode shown in Fig. 5 and Fig. 7. In particular, the three typical states resulting from external optical injection into the side modes discussed earlier are not clearly discernible in this case. Instead, injection into all side-modes shows a much more gradual progression toward the dual-mode state, with significant fluctuations in the two-mode intensity-difference between the Bragg mode and the injected side-mode.

These fluctuations, particularly noticeable just above threshold between 19 mA and 20 mA, were observed to cause the dual-mode characteristics to appear jagged and irregular, as opposed to the smooth, S-shaped profiles seen in Fig. 5. In particular, a careful analysis of the data in Table III and the associated plots suggests that injection into the three side-modes on the lower wavelength side of the Bragg mode showed more drastic fluctuations than injection into the three side-modes on the longer wavelength side. Furthermore, a second type of instability that was found to occur frequently for the more energetic side-modes was a “drifting” of the detuning condition. For instance, if the detuning between the injected ML signal and the slave side-mode was initially set to  $\Delta f = 0$  nm, it was often found after a few minutes that the detuning between the ML and the injected side-mode would spontaneously drift to  $\Delta f = \pm 0.002$  nm. This meant that the detuning condition had to be continuously monitored during the experiment, and restored back to the zero-detuning condition whenever it was found to have changed.

#### 4. DISCUSSION AND ANALYSIS

Based on the results presented in the previous section, two broad trends can be inferred – i.) the threshold condition for the Dual-Mode laser is directly related to the threshold condition for the solitary device; the lower the threshold of the solitary device, the lower the threshold of the Dual-Mode laser and the better the dual-mode characteristics, and ii.) strong intermodal background noise and a fluctuating mode structure in the solitary device yield significantly degraded threshold characteristics, even under strong optical injection. While the former might be quite obvious, considering that injection into a particular side-mode requires the establishment of a stable mode structure, so that the onset of the dual-mode threshold will necessarily follow the onset of lasing in the solitary device, the latter trend requires further discussion. To this end, the mode-patterns of the solitary devices offer further insight.

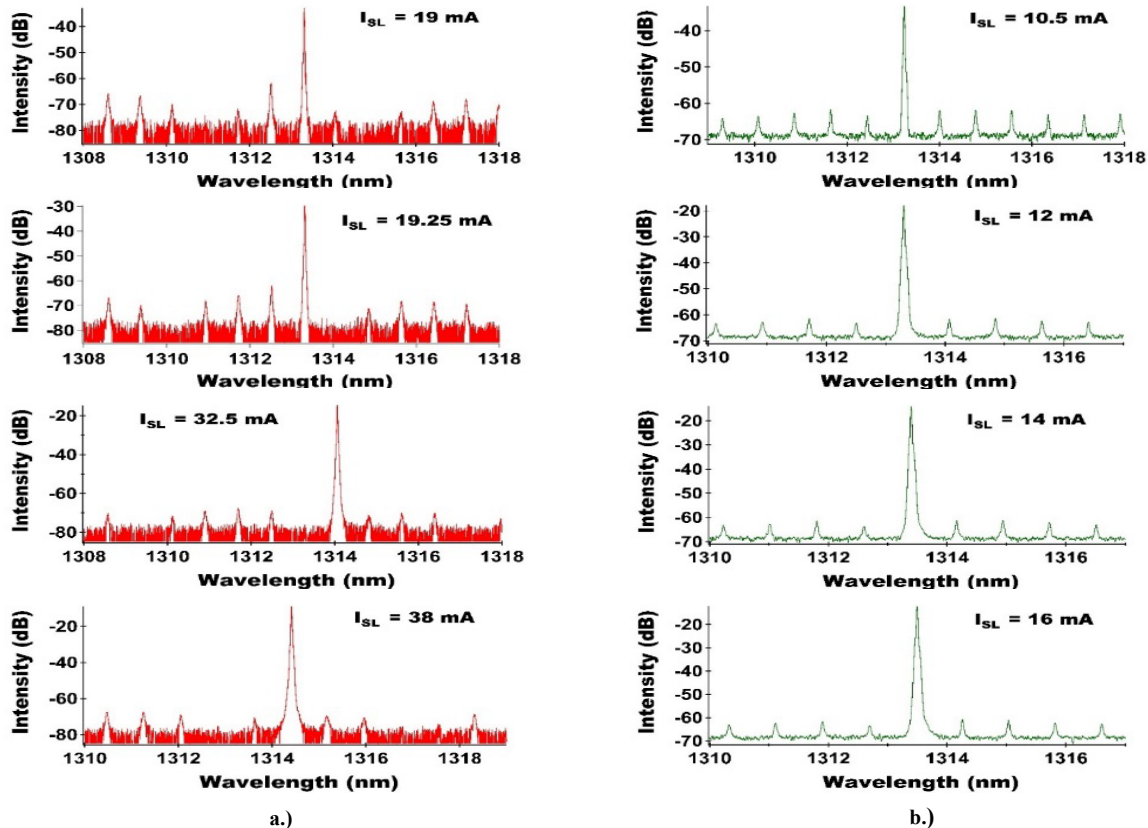


**Fig. 10:** Above-threshold evolution of solitary optical spectra with bias current, a.) QD-DFB #2 (red spectra) and b.) QD-DFB #1 (green spectra). Note the significantly more stable mode-structure and a much lower inter-modal noise floor for QD-DFB #1 with increasing bias current. All spectra recorded at an operating temperature of 64°C.

The graphic on the left (red spectra) of Fig. 10 shows the evolution of the optical spectrum of QD-DFB #2 at 64°C in solitary operation. The mode structure can be seen to be highly unstable in this case, with the shape and intensity of the side-modes undergoing a considerable transformation from frame-to-frame. For instance, the side-modes on the lower wavelength side nearest to the central Bragg mode can be seen to be more intense near threshold than the corresponding side-modes on the long wavelength side. The third side-mode on the shorter wavelength side of the Bragg mode is initially suppressed below the noise floor at 19 mA, but appears prominently at 19.25 mA. By comparison, the first three side-modes on the long wavelength side appear much weaker at 19 mA, and the second side-mode is completely suppressed. However, as the SL bias is raised to 19.25 mA, the first side-mode on the long wavelength side disappears, while the second side-mode appears with similar structure and intensity.

Well-above threshold, the situation is much different, as seen from the last two spectra corresponding to 32.5 mA and 38 mA, respectively. With the intensification of the lasing (Bragg) mode, all other residual modes are suppressed to approximately the same level around -70 dB. However, the significant background noise for this device results in the intermittent suppression of the weaker side-modes, so that instabilities continue to persist. The solitary spectra for QD-DFB #1 at the same operating temperature are shown alongside on the right in Fig. 10b.), for comparison. In stark contrast to the spectral evolution of QD-DFB #2, the mode-structure in this case is very stable with increasing slave bias. The threshold current in this case was much lower at 10.5 mA (nearly half that of QD-DFB #2 at the same temperature), so that the intracavity buildup of amplified spontaneous emission is much lower than for the second device. This is evidenced by the significantly lower noise floor between the side-modes.

In view of these observations, the role of side-mode structure and intensity (particularly the side-mode being injected) and intracavity noise in determining Dual-Mode characteristics is apparent. Numerous excellent theoretical and experimental efforts in the past have been devoted to studying the influence of side-mode structure on the optical linewidth of the lasing mode.<sup>15-17</sup> In this connection, it has been previously shown that the side-mode power strongly influences the linewidth of the dominant Bragg mode in a DFB laser, owing to mode-partitioning of noise, corresponding to the different longitudinal intensity distributions of the lasing mode, relative to the residual Fabry-Perot modes in such a device.<sup>15,16</sup> This coupling between the lasing and non-lasing modes of a DFB laser means that the more intense a side-mode (lower side-mode suppression ratio or SMSR relative to Bragg mode), the higher the fraction of noise partitioned into the mode. Furthermore, in ref. 16, side-modes located on the short wavelength side of the Bragg mode were found to have an asymmetric impact on the optical linewidth of the lasing (Bragg) mode, so that the linewidth of the lasing mode was found to be more sensitive to side-modes on the short wavelength side.

The results obtained in this work can be generally interpreted in terms of these findings. Firstly, the drastic fluctuations observed in the dual-mode characteristics for QD-DFB #2 just above the solitary device threshold are likely a direct consequence of the strong suppression of the Bragg mode by injection from the ML at these bias conditions. The strongly-suppressed Bragg mode, which is still more intense than the other side-modes (as seen in Fig. 4c), is now highly susceptible to intracavity noise, considering that a much higher fraction of the total intracavity noise is partitioned into this mode compared to the other side-modes. Thus, any fluctuations in the intracavity noise result in drastic fluctuations in its intensity, and thus, the peak-separation, ( $P_{inj} - P_{bragg}$ ). This would also explain the greater degree of fluctuations caused by injection into the three shorter wavelength side-modes in QD-DFB #2 (Fig. 9), considering that their greater intensity compared to the three longer wavelength side-modes would cause a greater fraction of the total intracavity noise partitioned into them. Furthermore, the intensity fluctuations in the side-modes have been proposed to instigate carrier-density fluctuations.<sup>17</sup> It is then conceivable that such carrier density fluctuations could, in turn, cause localized refractive index variations, and consequently, small wavelength shifts that could then cause the Master-Slave detuning condition to drift out of lock. This, however, remains the subject of further investigation.

## 5. CONCLUSIONS

In this work, dual-mode lasing characteristics have been analyzed for a 1310 nm QD-DFB laser subjected to external optical injection from a tunable, narrow linewidth cw source. The tunable range of this source was restricted to a total of six side-modes, so that two separate cases were investigated: i.) injection into six successive side-modes on the long wavelength side of the Bragg mode, and ii.) injection into the three successive side-modes closest to the Bragg mode, on either side of it. To ensure the same conditions for each injected side-mode, the power injected into the SL mode was held fixed at 1 mW, while the wavelength/frequency detuning condition between ML and SL was fixed at zero. The experiments were performed on two similarly-fabricated samples, QD-DFB #1 and QD-DFB #2.

Based on the findings of this study and the measured dual-mode characteristics for the two devices, it would appear that for the first few side-modes (within 5 nm) on either side of the Bragg mode, the structure of the side-mode being injected and its intensity, as well as the intracavity noise play a much more critical role in determining the dual-mode characteristics than the position of the mode relative to the Bragg mode.

More generally, it was found that stable dual-mode lasing characteristics require a low noise cavity, with well-suppressed side-modes and a low intermodal noise floor, even under strong optical injection. Fluctuations in side-mode intensity lead to instabilities such as fluctuations in the relative intensities of the two modes, and a “drifting” of the Master-Slave detuning condition. The findings of this work provide an important design guideline for the slave laser – a low threshold cavity with a high SMSR and a low noise floor is imperative toward achieving a stable, low noise, high power Dual-Mode source for precision RF-Photonic applications. In addition, future work could also potentially investigate the use of Nonlinear Dynamical techniques to reveal operating points with a reduced sensitivity to the systemic fluctuations discussed here.<sup>18</sup>

## ACKNOWLEDGEMENTS

The authors acknowledge the support of this work in part by the US Air Force under the Educational Partnership Agreement Number 14-283-RY-01. R. Raghunathan gratefully acknowledges continued support from the 2014 “Research in Paris” Postdoctoral Fellowship grant awarded by the City of Paris, France. V. Kovanis thanks the Electromagnetics Portfolio of Dr. Arje Nachman of AFOSR and acknowledges support by the Ministry of Education and Science of Kazakhstan.

Sadly, one of our co-authors, Justeen Olinger, passed away in November 2014 shortly after completing her experimental contribution to this paper. The Virginia Tech community has lost one of its brightest stars, a young woman with an infectious smile who will be dearly missed.

## REFERENCES

- [1]. Schneider, G. J., Murakowski, J. A., Schuetz, C. A., Shi, S. and Prather, D. W., “Radiofrequency signal-generation system with over seven octaves of continuous tuning,” *Nat. Photonics*, vol. **7**, 118–122 (2013).
- [2]. Van Dijk, F., Charbonnier, B., Constant, S., Enard, A., Fedderwitz, S., Formont, S., Lealman, I. F., Lecoche, F., Lelarge, F., Moodie, D., Ponnampalam, L., Renaud, C., Robertson, M. J., Seeds, A. J., Stohr, A. and Weiss, M., “Quantum dash modelocked lasers for millimeter wave signal generation and transmission”, in *Proc. 23rd Annu. Meeting IEEE Photon. Soc.*, 187–188 (2010).
- [3]. Shen, P., Gomes, N. J., Davies, P. A., Huggard, P. G. and Ellison, B. N. Analysis and demonstration of a fast tunable fiber-ring-based optical frequency comb generator. *J. Lightwave Technol.* **25**, 3257–3264 (2007).
- [4]. Fice, M. J., Rouvalis, E., Van Dijk, F., Accard, A., Lelarge, F., Renaud, C., Carpintero, G. and Seeds, A. J., “146-GHz millimeter wave radio-over-fiber photonic wireless transmission system”, *Opt. Exp.* **20**, 1769-1774 (2012).
- [5]. Laperle, C., Svilans, M., Poirier, M. and Tetu, M., “Frequency multiplication of microwave signals by sideband optical injection locking using a monolithic dual wavelength DFB laser device”, *IEEE Trans. Microwave Theory Tech.* **47**, 1219–1224 (1999).

- [6]. Braun, R. P., Grosskopf, G., Rohde, D. and Schmidt, F., “Low-phase-noise millimeter-wave generation at 64 GHz and data transmission using optical sideband injection locking”, *IEEE Photon. Technol. Lett.* **10**, 728–730 (1998).
- [7]. Hurtado, A., Henning, I.D., Adams, M. J., and Lester, L. F., “Dual-mode lasing in a 1310-nm quantum dot distributed feedback laser induced by single-beam optical injection”, *Appl. Phys. Lett.*, **102**(20), 201117-1–201117-4 (2013).
- [8]. Hurtado, A., Mee, J. K., Nami, M., Henning, I. D., Adams, M. J., and Lester, L. F., “Tunable microwave signal generator with an optically-injected 1310nm QD-DFB laser”, *Opt. Exp.*, **21**(9),10772–10778 (2013).
- [9]. Hurtado, A, Henning, I. D., Adams, M. J., and Lester, L.F., “Generation of Tunable Millimeter-Wave and THz Signals With an Optically Injected Quantum Dot Distributed Feedback Laser”, *IEEE Photonics Journal*, **5**(4), 5900107-5900107 (2013).
- [10]. Mee, J. K., Raghunathan, R., Wright, J. B., and Lester, L. F., “Device geometry considerations for ridge waveguide quantum dot mode-locked lasers”, *J. Phys. D: Appl. Phys.*, **47**(23), 233001 (2014).
- [11]. Liu, G. T., Stintz, A., Li, H., Malloy, K. J., and Lester, L. F., “Extremely low room-temperature threshold current density diode lasers using InAs dots in  $\text{In}_{0.15}\text{Ga}_{0.85}\text{As}$  quantum well”, *Electron. Lett.* **35**(14), 1163-1165 (1999).
- [12]. Berg, T. W. and Mork, J., “Quantum dot amplifiers with high output power and low noise”, *Appl. Phys. Lett.* **82**, 3083-3085 (2003).
- [13]. Su, H. and Lester, L. F., “Dynamic properties of quantum dot distributed feedback lasers: high speed, linewidth and chirp”, *J. Phys. D: Appl. Phys.* **38**, 2112 (2005).
- [14]. Zhang, L., Wang, R., Zou, Z., Gray, A., Olona, L., Newell, T. C., Webb, D., Varangis, P., and Lester, L. F., "InAs quantum dot DFB lasers on GaAs for uncooled 1310 nm fiber communications", Paper FG2, OFC 2003, March 2003, Atlanta, GA, USA.
- [15]. Henry, C. H. , Henry, P. S., and Lax, M. "Partition fluctuations in nearly single-longitudinal-mode lasers", *J. Lightwave Technol.* **LT-2**, 209 -216 (1984).
- [16]. Öberg, M. G., Broberg, B., Nilsson, S., Backbom, L., Morner, A., -C., Eriksson, G., Lundgren, L. and Vuorela, T., "Linewidth dependence on side-mode suppression in three-electrode DFB laser", *Electron. Lett.* **25**, 168-169 (1989).
- [17]. Yamada, M., “Theoretical analysis of line-broadening due to mode competition and optical feedback in semiconductor injection lasers”, *Trans. ZEICE*, **E71**, 152-160 (1988).
- [18]. Simpson, T. B., Liu, J.-M., AlMulla, M., Usechak, N. G., and Kovanis, V., “Limit-cycle dynamics with reduced sensitivity to perturbations”, *Phys. Rev. Lett.* **112**, 023901 (2014).